Resveratrol contributes to the inhibition of liver fibrosis by inducing autophagy via the microRNA-20a-mediated activation of the PTEN/PI3K/AKT signaling pathway

LILI ZHU[1*], QIUJU MOU[2*], YINGHUI WANG[3], ZIXIN ZHU[3] and MINGLIANG CHENG[4]

[1]Department of Blood Transfusion, The Affiliated Hospital of Guizhou Medical University;
[2]Department of Blood Transfusion, The Affiliated Baiyun Hospital of Guizhou Medical University;
[3]Graduate School, Guizhou Medical University; [4]Department of Infectious Diseases,
The Affiliated Hospital of Guizhou Medical University, Guiyang, Guizhou 550004, P.R. China

Received December 3, 2019; Accepted September 2, 2020

DOI: 10.3892/ijmm.2020.4748

Abstract. Liver fibrosis (LF) is a healing response to wounds resulting in liver injury that can cause liver failure or even cancer without functional prevention. Resveratrol (RSV) has been suggested to exert biological effects against various human diseases. MicroRNA-20a (miRNA/miR-20a) has been shown to promote disease progression. The present study aimed to assess the mechanisms through which RSV induces autophagy and activates the miR-20a-mediated phosphatase and tensin homolog (PTEN)/PI3K/AKT signaling pathway in LF. First, a rat model of carbon tetrachloride (CCL_4)-induced LF and a cell model of platelet-derived growth factor (PDGF)-BB-stimulated HSC-T6 cells were established for use in subsequent experiments. Subsequently, RSV at a range of concentrations was injected into the model rats with LF. Indicators related to liver injury, oxidative stress and fibrosis were determined in the rats with LF. The RSV-treated HSC-T6 cells were subjected to transfection with miR-20a mimic and PTEN overexpression plasmid to assess the levels of liver injury and LF. A dual-luciferase reporter gene assay was performed to verify the binding sites between PTEN and miR-20a. RSV was found to alleviate LF in rats, and autophagy was enhanced in the rats with LF following RSV treatment. Furthermore, the activation of the PTEN/PI3K/AKT axis attenuated LF, which was reversed by transfection with miR-20a mimic. RSV reversed the inhibitory effects of miR-20a on PTEN expression, reducing miR-20a expression and promoting PTEN, PI3K and p-AKT protein expression, thus attenuating LF. On the whole, the present study demonstrates that RSV induces autophagy and activates the miR-20a-mediated PTEN/PI3K/AKT signaling pathway to attenuate LF. These findings may lead to the development of potential therapeutic strategies for LF.

Correspondence to: Professor Mingliang Cheng, Department of Infectious Diseases, The Affiliated Hospital of Guizhou Medical University, 28 Guiyi Street, Guiyang, Guizhou 550004, P.R. China
E-mail: chengml08201@163.com

*Contributed equally

Key words: liver fibrosis, resveratrol, microRNA-20a, phosphatase and tensin homolog, PI3K/AKT signaling pathway

Introduction

Liver fibrosis (LF), which results from the overaccumulation of liver stellate cells and extracellular matrix by continuous hepatocellular injury and inflammatory reactions, is a main cause of the incidence and mortality rates of patients with liver-related diseases (1,2). Moreover, LF at an advanced stage leads to cirrhosis with architecture and attendant functional loss and eventually causes lethal complications (3). LF is mostly triggered by viral infection, but can also be triggered by alcoholism, chronic cholangiopathy, autoimmune hepatitis and obesity (4). Currently, LF is mainly diagnosed by non-invasive diagnostic methods, such as magnetic resonance imaging techniques and ultrasonography (5). Additionally, liver biopsy has failed to be effective for LF staging and diagnosis due to sampling uncertainty, possible pain and high patient reluctance (6). Moreover, current effective treatments for LF are limited only to the removal of the potential etiology and liver transplantation (7). Novel therapeutic strategies for LF thus are thus urgently required.

Resveratrol (RSV) is associated with different signaling pathways and immune responses due to its significant anti-inflammatory effects and oxidation resistance (8). In a recent study, RSV was found to strengthen liver function and block oxidative stress, thus alleviating LF (9). RSV relieves LF by inducing autophagy (10). Phosphatase and tensin homolog is highly involved in disease pathogenesis and the intracellular axis, rendering it an indispensable biomarker in a number of human diseases (11). PTEN has been found to hinder hepatic stellate cell (HSC) activation during LF (12). The regulation of PTEN in LF is tightly bound to autophagy (13). PTEN also affects the downstream PI3K/AKT signaling pathway and thus plays an essential role in LF (14). It has been previously

demonstrated that RSV hinders HSC activation to obstruct LF by inhibiting the PI3K/AKT signaling pathway (15,16). The PI3K/PTEN/AKT axis has been found to be related to the induction of autophagy in liver-associated disorders (17). miR-20a expression has been shown to be markedly increased in patients with LF (18). Furthermore, a negative correlation between miR-20a and PTEN has been found in liver diseases (19). It is also evident that RSV can attenuate the inhibitory effects of miR-20a on PTEN (20). From the above, it is thus reasonable to hypothesize that RSV, the PTEN/PI3K/AKT signaling pathway and miR-20a interact in LF. Thus, the present study conducted a series of experiments to verify this hypothesis.

Materials and methods

Ethics statement. The present study was approved and supervised by the Ethics Committee of the Affiliated Baiyun Hospital of Guizhou Medical University (Approval no. 2019-064). Each step in this experiment was approved by the laboratory animal ethics committee.

Model establishment and animal grouping. A total of 60 healthy adult male Sprague-Dawley rats [6-8 weeks old, weighing 250±30 g; Guangzhou University of Traditional Chinese Medicine; SYXK (Guangdong) 2018-0182] were adaptively raised in a room with 50-60% humidity at 20-24˚C with free access to food and water for 1 week prior to being used in the following experiments.

The rats were arranged by body weight and randomly assigned into the following groups of 12 rats each: i) The normal group; ii) LF (model) group; iii) low-dose RSV (L) group (treated with 40 mg/kg RSV); iv) medium-dose RSV (M) group (treated with 120 mg/kg RSV; and v) the high-dose RSV (H) group (treated with 200 mg/kg RSV). The doses of RSV used were according to relevant studies (21-24).

Apart from the rats in the normal group, which were injected with 1 ml/kg peanut oil, the rats in the other groups were intraperitoneally injected with a 1:1 mixture of 1 ml/kg carbon tetrachloride (CCL_4) and peanut oil 3 times a week for 6 weeks. Beginning at the end of the 6th week, the rats were injected once a week for 4 weeks. Beginning at the end of the 6th week, the rats in the RSV group were treated with RSV (R8350, Beijing Solarbio Science & Technology Co., Ltd.) by gavage following an intraperitoneal injection of CCL_4 once a day for 4 weeks. During the experiment, the behaviors and health of the animals were monitored by observing their diet, defecation and changes in weight every day.

Animal treatment and tissue sample collection. The experiment was performed based on the ARRIVE checklist (https://www.nc3rs.org.uk/arrive-guidelines). At the end of the 10th week, 24 h after the final dose, 1% pentobarbital sodium (45 mg/kg) was intraperitoneally injected to anaesthetize the rats. Rat blood (1 ml) was then routinely collected and centrifuged at 4˚C at 3,000 x g for 15 min to separate the serum, which was saved at -20˚C for further use. All 60 rats were then euthanized by an intraperitoneal injection of 800 mg/kg pentobarbital sodium (25), and the death of the rats was confirmed by observing that there was no fluctuation in the chest cavity (respiratory arrest) and no breathing and heartbeat sound (cardiac arrest) using a stethoscope. Subsequently, the rats were placed on ice for the immediate collection of liver tissues. Liver tissue homogenates were obtained from 3 rats in each group and stored at -80˚C for use in subsequent experiments. Liver tissues were prepared from another 3 rats from each group for observation using a transmission electron microscope (TEM). Tissues from the same liver regions of the remaining 6 rats were fixed with 10% formaldehyde to prepare paraffin-embedded sections for tissue staining.

Detection of alanine aminotransferase (ALT), aspartate aminotransferase (AST) and albumin (ALB) levels. The previously prepared serum samples stored at -20˚C were removed and allowed to thaw at room temperature. The supernatant was then retained after the samples were centrifuged at 3,000 x g at 4˚C for 10 min. ALT, AST and ALB levels in rat serum were then detected with a kit in accordance with the manufacturer's instructions (Nanjing Jiancheng Bioengineering Institute).

Detection of laminin (LN), hyaluronic acid (HA), procollagen (PC)-III and collagen type 1 (COL-1) levels. After serum samples and supernatants were obtained following the treatments described above, the LN, HA, PC-III and COL-1 levels in the rats were examined in accordance with the instructions of the ELISA kits (Shanghai ML Biotech Co., Ltd.).

Detection of hydroxyproline (HYP), malondialdehyde (MDA) and superoxide dismutase (SOD) levels. Following a wash in normal saline, 1 g of fresh liver tissue was ground into tissue homogenate and centrifuged at 3,000 x g at 4˚C for 10 min. The supernatant was then retained, and HSC-T6 cells were collected. The HYP, MDA and SOD contents in the liver tissue homogenate and cells were measured using HYP, MDA and SOD kits (Beijing Solarbio Science & Technology Co., Ltd.) in compliance with the manufacturer's instructions.

Reverse transcription-quantitative polymerase chain reaction (RT-qPCR). Total RNA was extracted using an RNA extraction kit (Takara Biotechnology Co., Ltd.), and the extracted RNA concentration was detected by measuring the absorbance at 260 nm. Total RNA was reverse transcribed into complementary DNA (cDNA) using a One StepPrimeScript miRNA cDNA Synthesis kit (Takara Biotechnology Co., Ltd.). The PrimeScript RT Reagent kit with gDNA Eraser (Takara Biotechnology Co., Ltd.) was used for reverse transcription of the mRNA. cDNA was used as the template, and the expression of each gene was detected by RT-qPCR with the SYBR Premix Ex Tap™ II kit (Takara Biotechnology Co., Ltd.) according to the manufacturer's instructions on a Roche LightCycler 480 (F. Hoffmann-La Roche Ltd.). The PCR thermocycling conditions were as follows: 95˚C for 3 min, followed by 40 cycles at 95˚C for 10 sec, 60˚C for 20 sec, and 72˚C for 40 sec. U6 was used as the internal reference for miR-20a, and β-actin was used as the internal reference for mRNA levels. The $2^{-\Delta\Delta Cq}$ method was used to calculate the expression levels (26). The sequences of the primers used for each gene are listed in Table I.

Western blot analysis. Total protein was extracted from the tissue homogenate and cells in each group using

Table I. Sequences of primers used for RT-qPCR.

Gene	Primers
miR-20a	F: 5'-TAAAGTGCTTATAGTGCAGGTAG-3'
	R: 5'-CTACCTGCACTATAAGCACTTTA-3'
U6	F: 5'-CGCTTCACGAATTTGCGTGTCAT-3'
	R: 5'-GCTTCGGCAGCACATATACTAAAAT-3'
PTEN	F: 5'-ACCAGTGGCACTGTTGTTTCAC-3'
	R: 5'-TTCCTCTGGTCCTGGTATGAAG-3'
α-SMA	F: 5'-GGCCCTAGCACCCAGCACCATGAA-3'
	R: 5'-CCGGCTTCATCGTATTCCTGTTT-3'
TGF-β1	F: 5'-ATTCCTGGCGTTACCTTGG-3'
	R: 5'-AGCCCTGTATTCCGTCTCCT-3'
TIMP-1	F: 5'-TTCGTGGGGACACCAGAAGTC-3'
	R: 5'-TATCTGGGACCGCAGGGACTG-3'
β-actin	F: 5'-GGCATGGGTCAGAAGGATTCC-3'
	R: 5'-ATGTCACGCACGATTTCCCGC-3'

miR, microRNA; PTEN, phosphate and tension homology deleted on chromsome ten; α-SMA, α-smooth muscle actin; TGF-β1, transforming growth factor-β1; TIMP-1, tissue inhibitor of metalloproteinase-1; F, forward; R, reverse.

radioimmunoprecipitation assay lysis buffer. The protein concentration was determined using the bicinchoninic acid method, and loading buffer was added for denaturation in a metal bath for 10 min at 100˚C. Samples containing the same amount of protein (30 g) were added to 10% sodium dodecyl sulfate-polyacrylamide gels. Following electrophoresis, the proteins were transferred onto polyvinylidene fluoride membranes. The membranes were blocked with 5% skim milk powder for 1 h and incubated with primary antibodies against the following (all from Abcam) at 4˚C overnight: α-smooth muscle actin (α-SMA; ab32575, 1:1,000), tissue inhibitor of metalloproteinase-1 (TIMP-1; ab38978, 1:1,000), transforming growth factor-β1 (TGF-β1; ab92486, 1 μg/ml), light chain (LC)3-I (ab51520, 1:3,000), LC3-II (ab48394, 1:200), Beclin1 (ab210498, 1:1,000), anti-thymocyte globulin (Atg)7 (ab52472, 1:100,000), p62 (ab91526, 1 μg/ml), COL-1 (ab96723, 1:500), PTEN (ab32199, 1:10,000) and p-AKT (ab8805, 1:500), PI3K (ab40776, 1:1,000). The membranes were incubated for 1 h with anti-rabbit immunoglobulin G (IgG; ab6728, Abcam, 1:2,000) labeled with horseradish peroxidase and then visualized for observation. β-actin (ab8226, Abcam, 1:1,000) was applied as the internal reference. Relative expression is represented by the ratio of the gray values for the target protein and internal reference. Image Pro Plus 6.0 (Media Cybernetics, Inc.) was used for densitometry.

Hematoxylin and eosin (H&E) staining. The paraffin-embedded sections were regularly dewaxed and stained with hematoxylin (Beijing Solarbio Science & Technology Co., Ltd.) at room temperature for 3 min. After washing, the sections were placed in hydrochloric acid and ammonium hydroxide for 2 sec. The sections were then washed with distilled water, stained with eosin at room temperature for 5 min and washed with distilled water again. Subsequently, the sections were dehydrated with gradient ethyl alcohol and cleared with xylene. Finally, the membranes were sealed by neutral resin and then tested by microscopy (BX60, Olympus Corporation). LF staging in rats was determined by the Knodell histology activity index system (27).

Masson's trichrome staining. The paraffin-emdedded sections were regularly dewaxed and stained with 100 μl of Masson's solution (Beijing Solarbio Science & Technology Co., Ltd.) for 5 min. The sections were then washed and then at room temperature stained with 100 μl of phosphomolybdic acid for 5 min. When the sections had dried, 100 μl of aniline blue was used to stain the sections at room temperature for 5 min. After being washed with distilled water, the sections were successively differentiated twice by incubation with 100 μl of tissue differentiation solution at room temperature for 40 sec each. The sections were dehydrated with 95% ethyl alcohol and anhydrous alcohol, permeabilized, sealed with neutral resin and examine under a microscope (BX60, Olympus Corporation).

Immunohistochemical staining. The paraffin-embedded sections were placed on anti-off slides and dried in a 60˚C oven for 4 h. After regular dewaxing and dehydration, the sections were incubated with a 3% H_2O_2 solution for 15 min at room temperature and then incubated with normal anti-goat serum for 15 min at room temperature for antigen retrieval. Primary antibodies (all from Abcam) against the following were added to the sections followed by incubation at 4˚C overnight: Beclin1 (ab210498, 1:100), Atg7 (ab52472, 1:500), α-SMA (ab5831, 5 μg/ml), COL-1 (ab3453, 1:500) and p-AKT (ab8805, 1:1,000). Following 3 washes in phosphate-buffered saline (PBS) for 3 min each, secondary antibody IgG (ab6721, 1:1,000) was mixed with the sections and incubated for 1 h at 37˚C before another 3 PBS washes for 3 min each. The sections were visualized with diaminobenzidine and counterstained with hematoxylin for 3-5 min at room temperature. Following regular dehydration, the dried sections were sealed in gum and then observed by microscopy (BX60, Olympus Corporation). A total of 5 visual fields were randomly selected from each section and used to calculate the ratio of positive cells among 100 cells.

TEM observation. Liver tissue sections at 1 mm^3 were fixed with 2% glutaraldehyde for 2 h. Following a buffer wash, the tissues were fixed with osmic acid and dehydrated with a series of acetone solutions for 5-15 min each. The liver tissues were soaked in a mixture of acetone and embedding medium for 2-4 h at room temperature, embedded in resin embedding medium, sliced and then stained with uranyl acetate and lead citrate for 15-30 min. Finally, the tissues were observed under a TEM (Philips CM10, Philips).

Cell culture and treatment. HSC-T6 cells were obtained from the Shanghai Cell Biochemistry Institute, Chinese Academy of Sciences. The cells were cultured in Dulbecco's modified Eagle medium supplemented with 10% fetal bovine serum and 1% penicillin/streptomycin in a 37˚C incubator with 5% CO_2. After reaching 70-80% confluency, the cells were sub-cultured.

Cells in the exponential growth phase were selected for use in subsequent experiments.

The HSC-T6 cells were assigned to the following groups: i) The control group, ii) platelet-derived growth factor (PDGF)-BB group [HSC-T6 cells were treated with 10 mg/ml PDGF-BB (P00031, Beijing Solarbio Science & Technology Co., Ltd.) for 48 h]; iii) PDGF-BB + RSV + L group (HSC-T6 cells were treated with 10 mg/ml RSV prior to the addition of PDGF-BB 48 h later); iv) PDGF-BB + RSV + M group (HSC-T6 cells were treated with 30 mg/ml RSV prior to the addition of PDGF-BB 48 h later); v) the PDGF-BB + RSV + H group (HSC-T6 cells were treated with 50 mg/ml RSV prior to the addition of PDGF-BB 48 h later). The HSC-T6 cells treated with 30 mg/ml RSV and PDGF-BB were further divided the following subgroups: i) The mimic negative control (NC) group (HSC-T6 cells were treated with 30 mg/ml RSV and PDGF-BB and transfected with mimic NC); ii) miR-20a mimic group (HSC-T6 cells were treated with 30 mg/ml RSV and PDGF-BB and transfected with miR-20a mimic); iii) miR-20a mimic + pcDNA3.1 group (HSC-T6 cells were treated with 30 mg/ml RSV and PDGF-BB and transfected with miR-20a mimic + pcDNA3.1); and iv) the miR-20a mimic + pcDNA3.1-PTEN group (HSC-T6 cells were treated with 30 mg/ml RSV and PDGF-BB and transfected with miR-20a mimic + pcDNA3.1-PTEN). The vectors were provided by Beyotime Institute of Biotechnology, Inc., miR-20a mimic and its NC were constructed and synthesized by Shanghai GenePharma Co., Ltd.. pcDNA3.1-PTEN and miR-20a mimic and its NC used for transfection were 100 nM and transfection was carried out using Lipofectamine™ 2000 (Invitrogen; Thermo Fisher Scientific, Inc.). The transfection efficacy was verified by RT-qPCR and western blot analysis 48 h later.

3-(4,5-Dimethylthiazol-2-yl)-2,5-diphenyltetrazolium bromide (MTT) assay. The HSC-T6 cells in the exponential growth phase were counted following detachment with trypsin. The cell suspension was diluted to $3x10^4$ cells/ml, and 200 μl of the cell suspension were seeded into each well of a 96-well plate. Subsequently, 10 mg/ml PDGF-BB and 10, 30 or 50 mg/ml RSV solution were added following cell adherence, with 6 parallel wells in each group. The control group was treated with the same volume of culture solution. This was followed by the addition of 20 μl of 5 mg/ml MTT (Beijing Solarbio Science & Technology Co., Ltd.) dissolved in PBS to the wells following 48 h of culture. Following 4 h of treatment in an incubator at 37˚C, the supernatant was discarded, and 150 μl of dimethyl sulfoxide were added to each well and shaken for 10 min. The optical density at a wavelength of 490 nm was measured using a microplate reader (BIO-RAD680, Bio-Rad Laboratories Inc.).

Dual-luciferase reporter gene assay. miRs targeting PTEN were detected using starBase (http://starbase.sysu.edu.cn/) and TargetScan (http://www.targetscan.org/vert_72/) software. The overlapping results of these 2 databases revealed specific binding sites between the 3'UTR of PTEN and miR-20a. pmirGLO vector (Shanghai GenePharma, Co., Ltd.) was utilized to establish wild-type (WT) PTEN plasmid (PTEN-WT) and mutant (MUT) PTEN plasmid (PTEN-MUT), which were separately mixed with mimic NC and miR-20a mimic and then Lipofectamine™ 2000 (Invitrogen; Thermo Fisher Scientific, Inc.) prior to transfection into 293T cells (China Center for Type Culture Collection). Finally, luciferase activity was assessed 48 h later. All the experiments were performed 3 times.

Statistical analysis. SPSS 21.0 (IBM Corp.) was employed for data analysis. The Kolmogorov-Smirnov test was used to indicate whether the data were normally distributed. The results are presented as the means ± standard deviation. One-way analysis of variance (ANOVA) or two-way ANOVA were used to compare different groups, and Tukey's multiple comparisons test was applied for pairwise comparisons following ANOVA. P-values were attained using a two-tailed test, and $P<0.05$ was considered to indicate a statically significant difference.

Results

RSV mitigates liver injury in rats with LF. To examine the effects of RSV on LF, a rat model of LF was established and the ALT, AST and ALB serum levels were detected in the rats. The results revealed that the ALT and AST serum levels in the rats with LF were markedly increased, while the ALB level was markedly decreased. The changes in ALT, AST and ALB serum levels in rats with LF were normalized by RSV treatment ($P<0.05$ and $P<0.01$; Fig. 1A). The LN, HA and PC-III levels in serum form the model rats, and the HYP and MDA levels in the liver tissue homogenate were elevated, while the SOD levels were decreased. Of note, RSV treatment reversed these outcomes (all $P<0.05$ and $P<0.01$; Fig. 1B and C). The results of H&E and Masson's staining results revealed that the liver tissues of rats in the normal group were complete with clearly visible cells. By contrast, the tissues from the rats in the model group exhibited loose and extending liver cells, portal necrosis, a disordered arrangement of the liver lobules, pseudolobuli formation, loose cytoplasm, massive collagen fiber hyperplasia, distant fibers and an enlarged collagen volume fraction (CVF). However, following treatment with low-, medium- and high-dose RSV, rat liver cell death was gradually alleviated, the liver lobule structure was normalized, and collagen fiber hyperplasia and CVF decreased ($P<0.05$ and $P<0.01$; Fig. 1D and E). Western blot analysis revealed that the protein expression of α-SMA, TIMP-1 and TGF-β1 in the tissues of rats with LF was higher than that in the tissues of rats in the normal group; however, these effects were reversed by treatment with RSV (all $P<0.05$ and $P<0.01$; Fig. 1F).

RSV induces hepatocellular autophagy in rats with LF. A previous study noted that hepatocellular autophagy plays an important role in LF (28). Thus, the present study used immunohistochemical staining to evaluate the expression of autophagy-related proteins in the liver tissues of rats in each group. It was found that the Beclin1 and Atg7 proteins were mainly present in the cytoplasm of the liver cells. Compared with that in the sham-operated rats, Beclin1 and Atg7 expression in the liver tissues of the model rats was significantly decreased. However, Beclin1 and Atg7 expression was enhanced following treatment with RSV at various doses ($P<0.05$ and $P<0.01$; Fig. 2A). Subsequently, the expression of autophagy-related proteins in the liver tissues of rats was detected by western blot analysis. It was found that compared with the control rats, the rats in the model group exhibited a

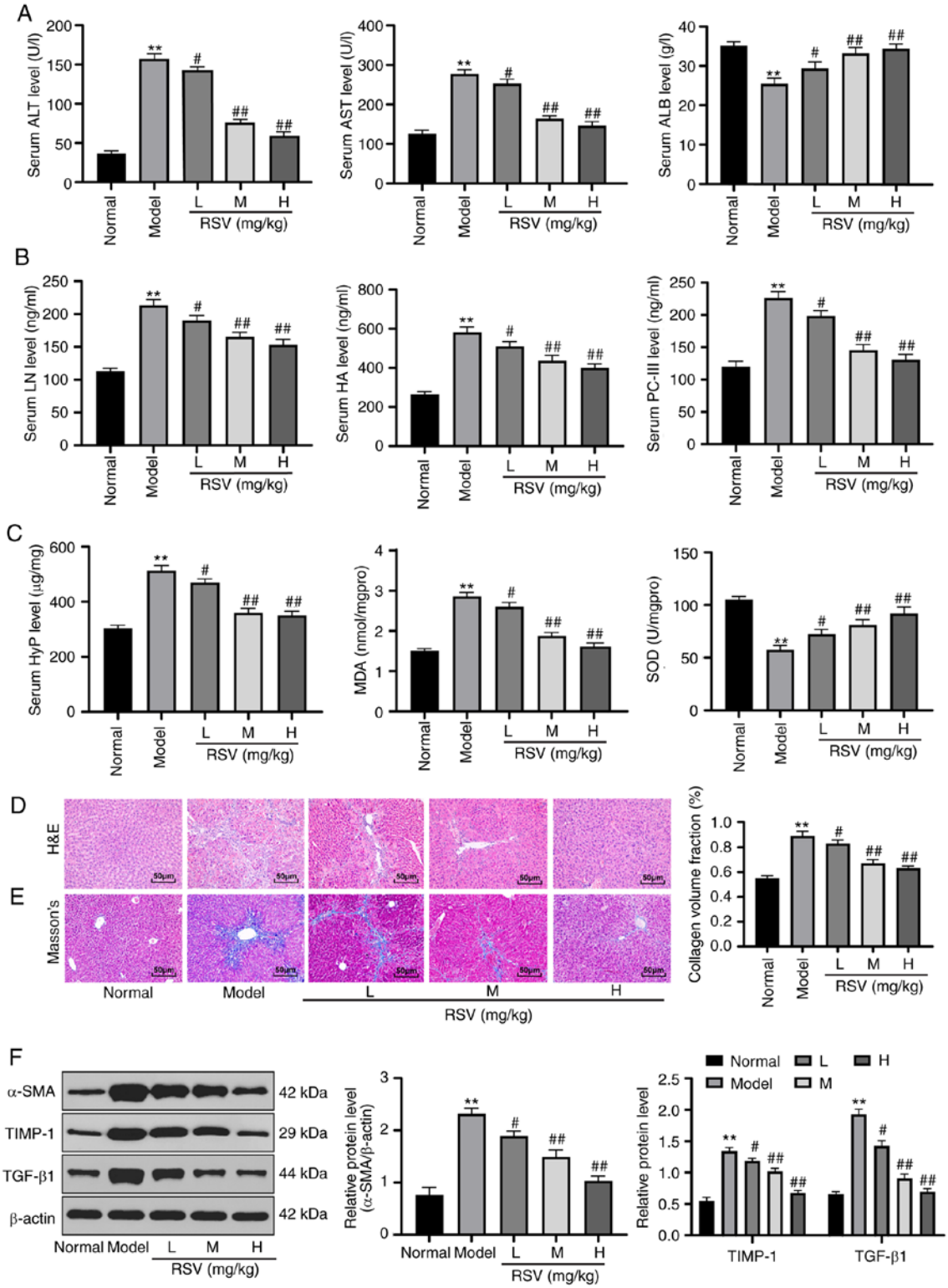

Figure 1. RSV mitigates liver injury in rats with LF. (A) Detection of ALT, AST and ALB levels in the sera of rats with LF; n=12 per group. (B) LN, HA and PC-III levels in the sera of rats with LF were measured with ELISA kits; n=12 per group. (C) HYP, MDA and SOD levels in liver tissue homogenates were verified using kits; n=3 rats per group. (D) H&E staining and (E) Masson's staining were employed to observe pathological changes in the liver tissues of rats in each group; magnification, x200, n=6 rats per group. (F) Western blot analysis was applied to assess α-SMA, TIMP-1 and TGF-β1 protein expression in the tissues of rats in each group. Each experiment was independently repeated 3 times. The data were analyzed by one-way ANOVA or two-way ANOVA, followed by Tukey's multiple comparisons test; **P<0.01, compared with the normal group; $^{\#}$P<0.05 and $^{\#\#}$P<0.01, compared with the model group. RSV, resveratrol; LF, liver fibrosis; ALT, alanine aminotransferase; AST, aspartate aminotransferase; ALB, albumin; LN, laminin; HA, hyaluronic acid; PC, procollagen; HYP, hydroxyproline; MDA, malondialdehyde; SOD, superoxide dismutase; ANOVA, analysis of variance.

decreased LC3-II/LC3-I ratio, a decreased Beclin1 and Atg7 protein expression and an increased p62 protein expression. Following treatment with RSV at various doses, autophagy in the rat liver tissues was promoted (P<0.05 and P<0.01;

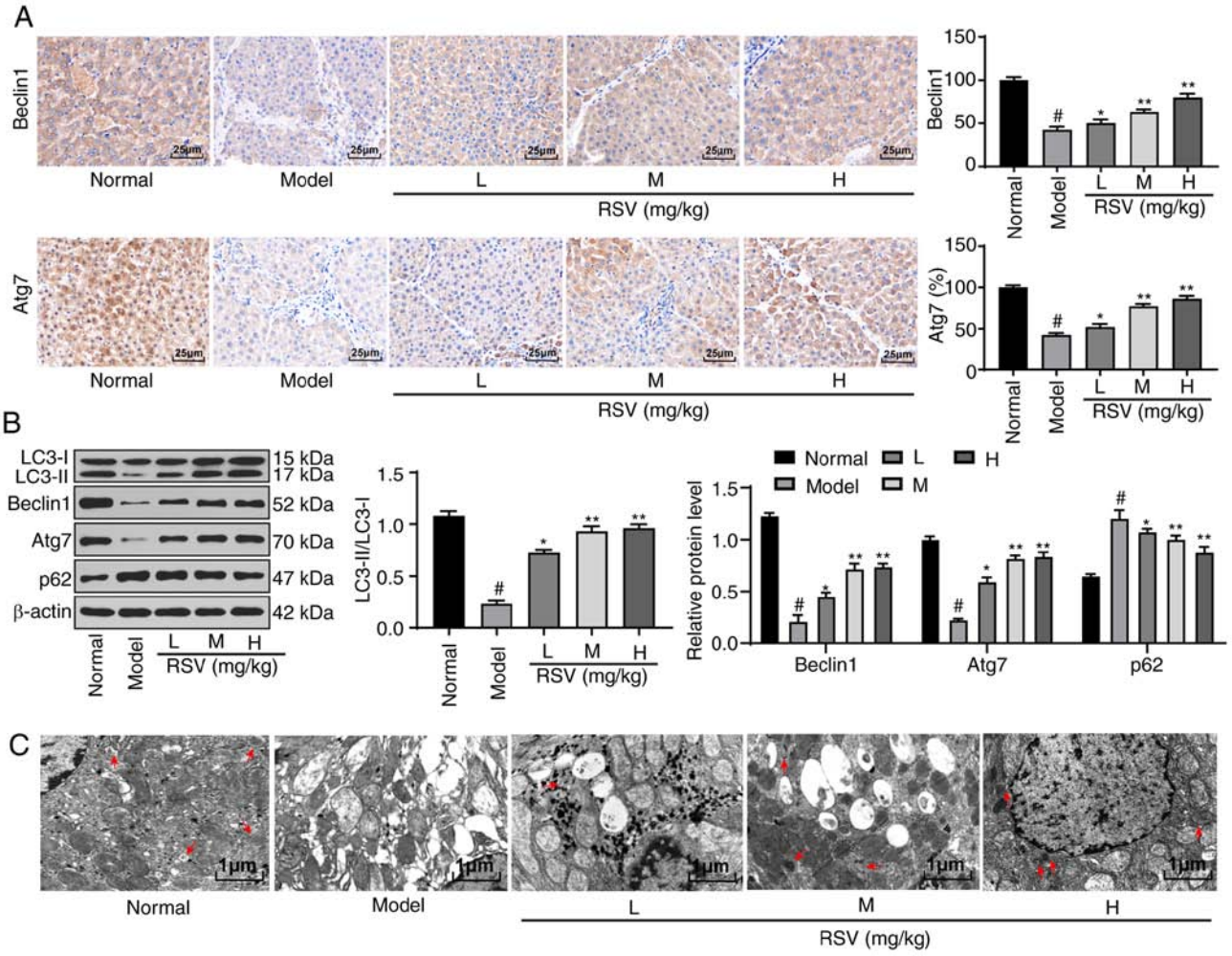

Figure 2. RSV induces autophagy in rats with LF. (A) Immunohistochemical staining was performed to detect Beclin1 and Atg7 protein expression in the liver tissues of rats with LF; magnification, x400, n=6 rats per group. (B) Western blot analysis was conducted to assess LC3-II, LC3-I, Beclin1, Atg7 and p62 protein expression in the liver tissues of rats from each group; n=3 rats per group. (C) TEM was used to observe autophagosomes in the liver tissues of rats in every group (as indicated by the arrow); magnification, 1,000, n=3 rats per group. Each experiment was independently repeated 3 times. The data were analyzed by one-way ANOVA or two-way ANOVA, followed by Tukey's multiple comparisons test; *P<0.05 and **P<0.01, compared with the model group; $^{\#}$P<0.05, compared with the normal group. RSV, resveratrol; LF, liver fibrosis; TEM, transmission electron microscopy; ANOVA, analysis of variance.

Fig. 2B). The autophagic flux is blocked through the inhibition of the fusion of autophagosomes and lysosomes, leading to aggravated liver damage (29). In the present study, observation by TEM revealed that there were fewer autophagosomes in the liver tissues of the model rats compared with the control rats, while the number of autophagosomes in the rat liver tissues increased with the increasing doses of RSV (Fig. 2C).

RSV alleviates LF by activating the PTEN/PI3K/AKT signaling pathway. A previous study indicated that PTEN affects the activation and apoptosis of HSCs in LF (30) and that PTEN exerts a specific effect on LF via the PI3K/Akt/STAT6 axis (31). Hence, it was hypothesized that RSV plays a role in inhibiting LF via the PTEN/PI3K/AKT axis. Subsequently, the mRNA and protein expression levels of PTEN in the liver tissues of rats in each group were detected by RT-qPCR and western blot analysis, respectively. It was found that PTEN mRNA and protein expression in rats in the model group was markedly reduced compared with the rats in the control group. The mRNA and protein expression levels of PTEN in the rats with LF treated with RSV at various doses were significantly increased in a dose-dependent manner (P<0.05 and P<0.01; Fig. 3A and B). Immunohistochemical staining then revealed few yellow granules in the control group, but clusters of brownish yellow granules in the model group. Compared with the model group, the granular brownish yellow substance in the RSV-treated groups decreased with the increasing RSV concentration (P<0.05 and P<0.01; Fig. 3C). Compared with those in the control group, the PI3K and p-AKT protein levels were increased in the model group, but were reduced in the RSV-treated groups (P<0.05 and P<0.01; Fig. 3D).

miR-20a suppresses PTEN expression. The above-mentioned results revealed that the PTEN/PI3K/AKT axis played a specific role in the rat model of LF. However, the upstream mechanism of the PTEN/PI3K/AKT axis remains unclear. Therefore, miRs containing PTEN-binding sites were predicted through starBase. It was found that a number of miRs, including miR-20a, contain PTEN-binding sites (Fig. 4A). miR-20a is a fibrosis-related miR (32). Hence, it was hypothesized that miR-20a may play a role in LF by regulating

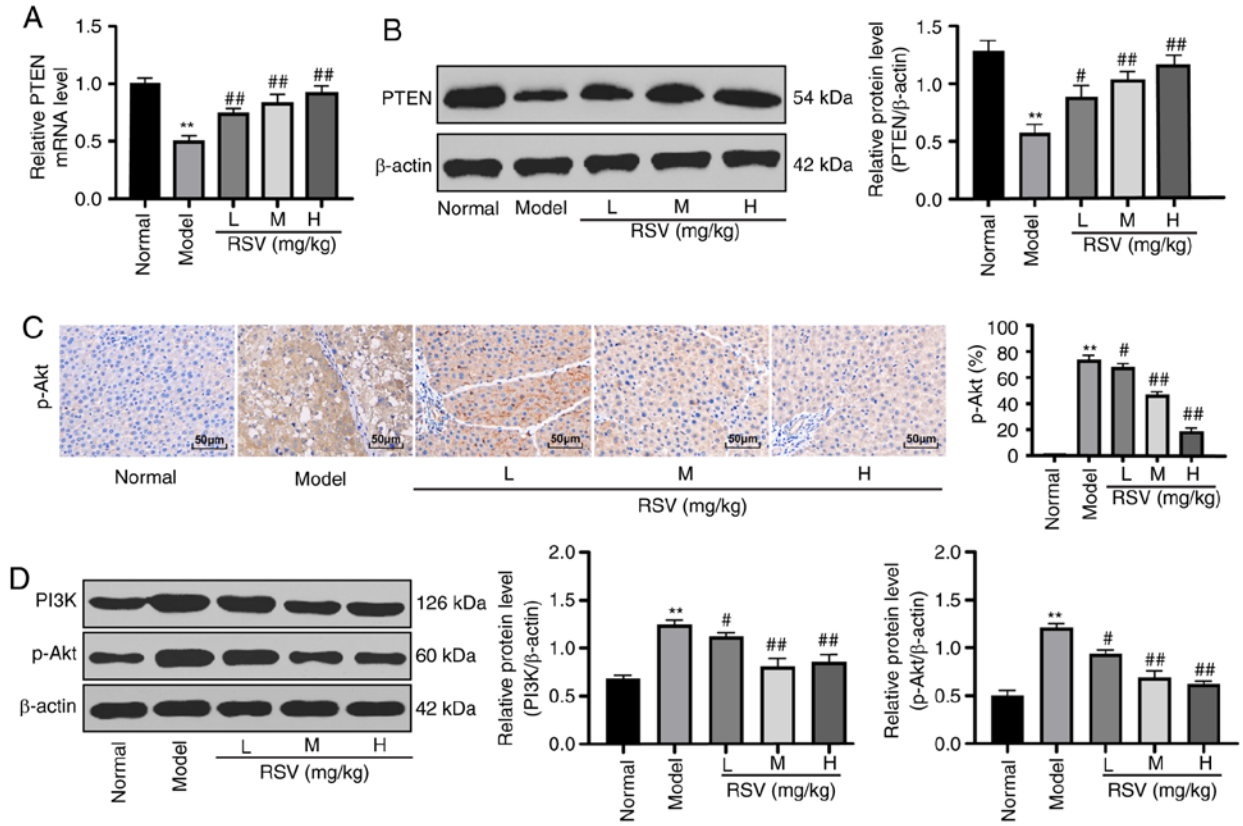

Figure 3. RSV alleviates liver injury in rats with LF by activating the PTEN/PI3K/AKT signaling pathway. (A and B) PTEN mRNA and protein expression in the liver tissues of rats with LF was verified with RT-qPCR and western blot analysis, respectively; n=3 rats per group. (C) p-AKT protein expression was measured by immunohistochemical staining; magnification, x400, n=6 rats per group. (D) PI3K and p-AKT protein expression in the liver tissues of rats with LF was detected by western blot analysis; n=3 rats per group. Each experiment was independently repeated 3 times. One-way ANOVA and Tukey's multiple comparisons test were applied for data analysis; **P<0.01, compared with the normal group; $^{\#}$P<0.05 and $^{\#\#}$P<0.01, compared with the model group. RSV, resveratrol; LF, liver fibrosis; mRNA, messenger RNA; RT-qPCR, reverse transcription-quantitative polymerase chain reaction; ANOVA, analysis of variance.

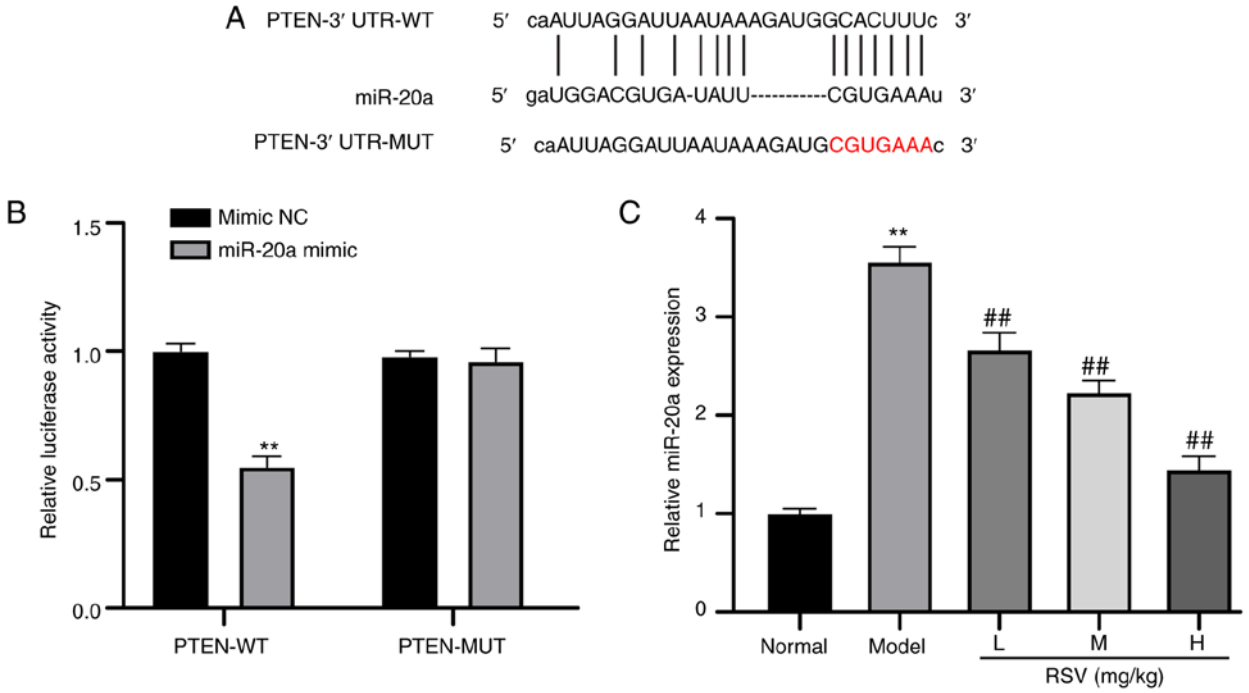

Figure 4. miR-20a suppresses PTEN expression. (A) starBase and TargetScan were employed to predict binding sites between the PTEN 3'UTR and miR-20a. (B) A dual-luciferase reporter gene assay was performed to confirm the target association between miR-20a and PTEN. (C) miR-20a expression in rat tissues was detected by RT-qPCR. Each experiment was independently repeated 3 times. Two-way ANOVA was applied to analyze the data in (B) one-way ANOVA was applied to analyze the data in (C) followed by Tukey's multiple comparisons test; **P<0.01, compared with the normal group; $^{\#\#}$P<0.01, compared with the model group. miR, microRNA; RT-qPCR, reverse transcription-quantitative polymerase chain reaction; ANOVA, analysis of variance; NC, negative control.

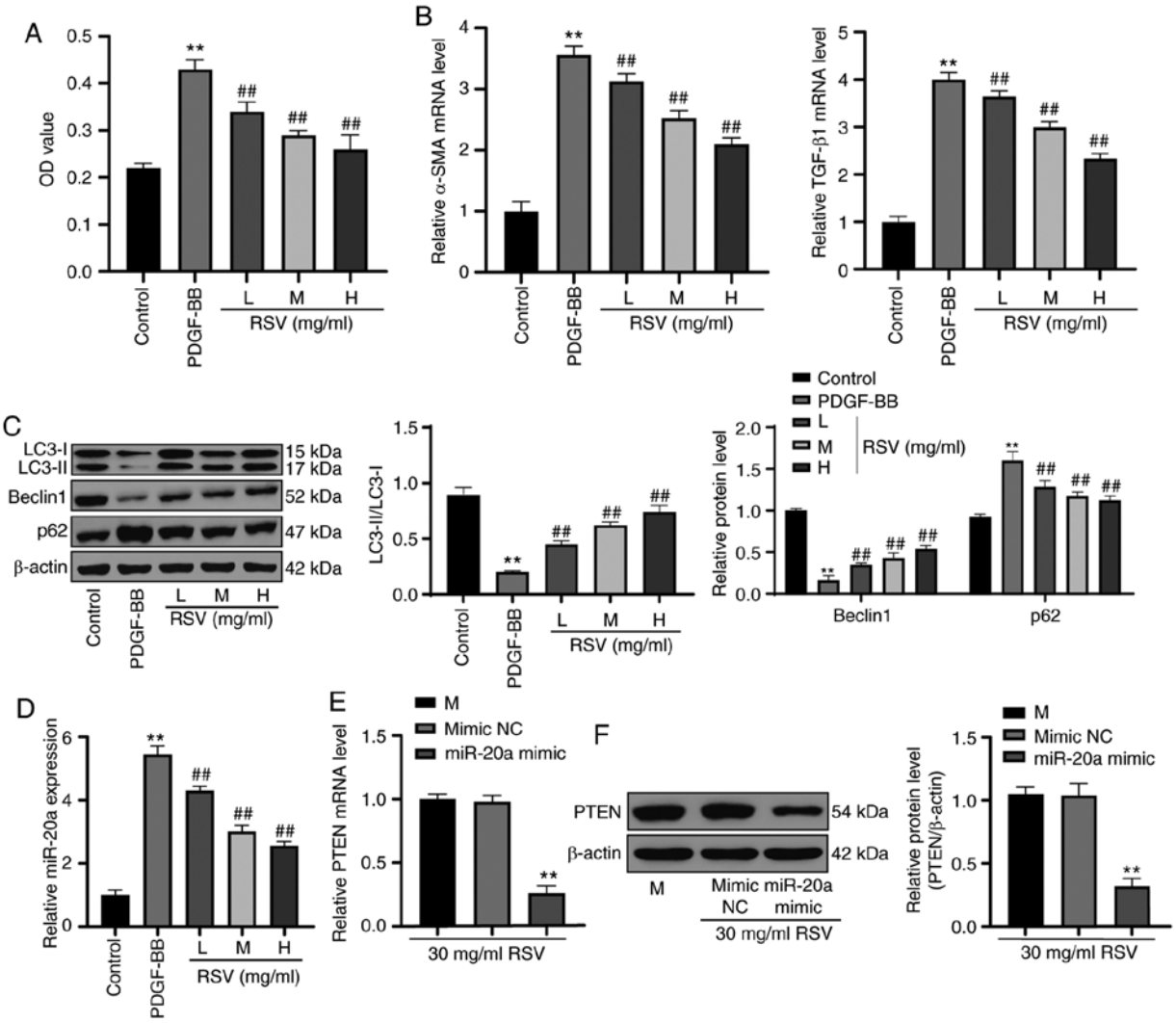

Figure 5. RSV promotes cell autophagy and decreases the inhibitory effect of miR-20a on PTEN. (A) HSC-T6 cell proliferation following RSV treatment was verified by MTT assay. (B) mRNA expression of α-SMA and TGF-β1 in HSC-T6 cells treated with RSV was detected by RT-qPCR. (C) Western blot analysis was used to detect autophagy-related protein expression. (D) miR-20a expression in HSC-T6 cells following treatment with RSV was measured by RT-qPCR. (E and F) After miR-20a was overexpressed, RT-qPCR and western blot analysis were performed to determine PTEN mRNA and protein expression, respectively in HSC-T6 cells treated with RSV. Each experiment was independently repeated 3 times. One-way ANOVA and Tukey's multiple comparisons test were applied to determine the statistical significance of the data; **P<0.01, compared with the control group and the mimic NC group; $^{\#\#}$P<0.01, compared with the PDGF-BB group. RSV, resveratrol; miR, microRNA; MTT, 3-(4,5-Dimethylthiazol-2-yl)-2,5-diphenyltetrazolium bromide; mRNA, messenger RNA; RT-qPCR, reverse transcription-quantitative polymerase chain reaction; ANOVA, analysis of variance; NC, negative control; PDGF, platelet-derived growth factor.

the PTEN/PI3K/AKT axis. Through a dual-luciferase reporter gene assay, it was found that the luciferase activity of the miR-20a mimic in cells expressing PTEN-WT was markedly decreased (P<0.01; Fig. 4B). Compared with that in the control group, miR-20a expression was higher in the model group, but was significantly decreased in the RSV-treated groups (P<0.01; Fig. 4C).

RSV promotes cell autophagy and decreases the inhibitory effects of miR-20a on PTEN. Following treatment with PDGF-BB, HSC-T6 cell viability was increased, and the mRNA expression of α-SMA and TGF-β1 was promoted. However, RSV at increasing concentrations gradually decreased HSC-T6 cell viability and decreased the mRNA expression of α-SMA and TGF-β1 (all P<0.01; Fig. 5A and B). Western blot analysis was used to detect autophagy-related indexes. The LC3-II/LC3-I ratio and Beclin 1 protein level were significantly decreased, and p62 protein expression was evidently increased. However, following treatment with RSV at increasing concentrations, the LC3-II/LC3-I ratio and Beclin 1 protein expression markedly increased, and p62 protein expression notably decreased (all P<0.01; Fig. 5C). miR-20a was actively expressed in HSC-T6 cells treated with PDGF-BB; however, its expression decreased following treatment with RSV at increasing concentrations (P<0.01; Fig. 5D). In activated HSC-T6 cells treated with 30 mg/ml RSV, the mRNA and protein expression of PTEN was significantly decreased following its upregulation by miR-20a (P<0.01; Fig. 5E and F).

RSV inhibited LF by downregulating miR-20a and modulating the PTEN/PI3K/AKT signaling pathway. When both miR-20a

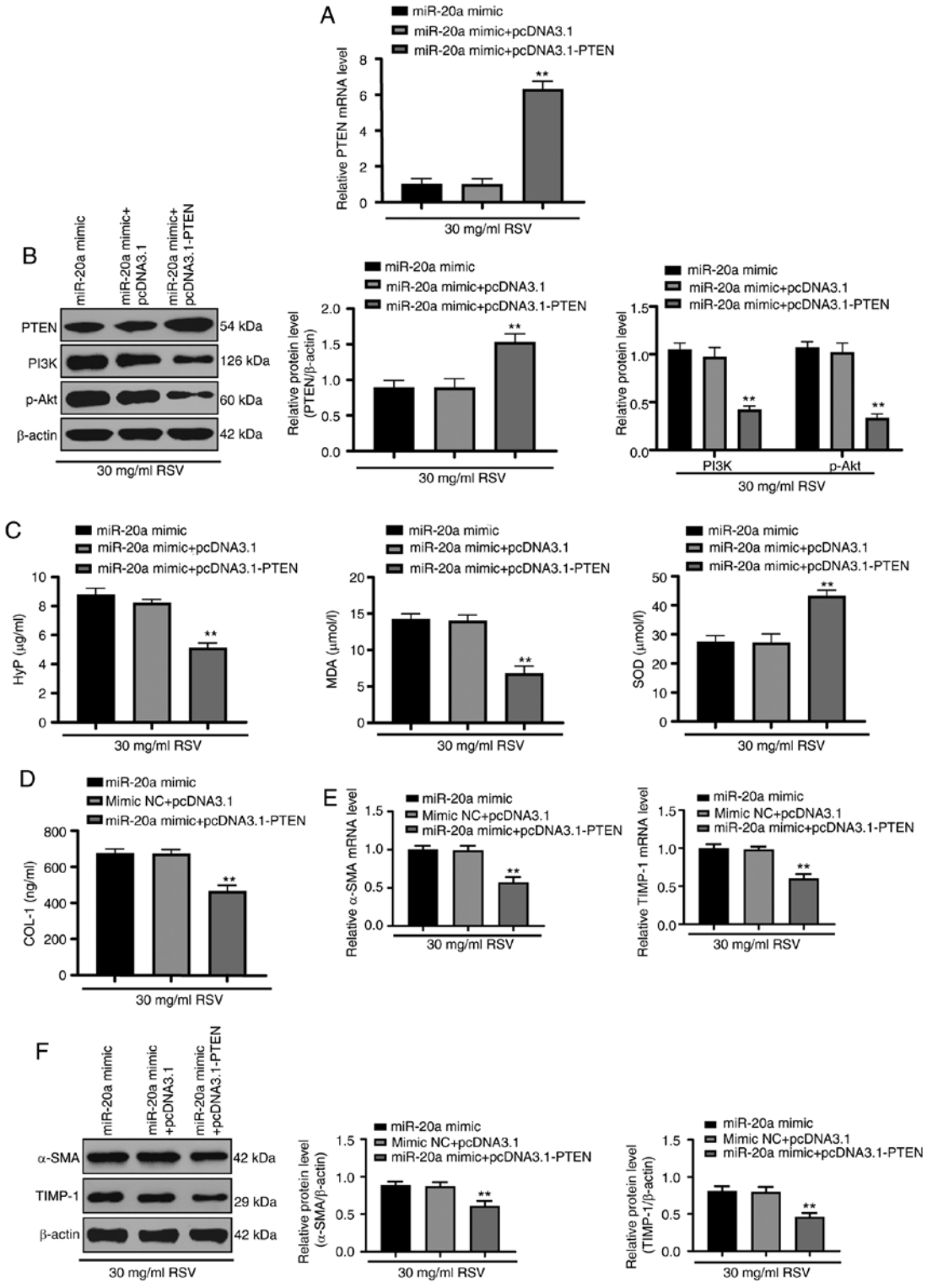

Figure 6. miR-20a promotes LF by activating the PTEN/PI3K/AKT signaling pathway. (A and B) RT-qPCR and western blot analysis were performed to determine PTEN mRNA and protein expression, respectively, in HSC-T6 cells and western blot analysis was performed to determine PI3K and p-AKT protein expression. (C) HYP, MDA and SOD levels in HSC-T6 cells were detected with a kit. (D) A kit was used to determine COL-1 protein levels in HSC-T6 cells. (E) The mRNA expression of α-SMA and TGF-β1 in HSC-T6 cells was assessed by RT-qPCR. (F) Western blot analysis was conducted to measure α-SMA and TIMP-1 protein expression in HSC-T6 cells. Each experiment was independently repeated 3 times. The data were analyzed by one-way ANOVA or two-way ANOVA, followed by Tukey's multiple comparisons test; **P<0.01, compared with the miR-20a mimic + pcDNA3.1 group. miR, microRNA; LF, liver fibrosis; RSV, resveratrol; mRNA, messenger RNA; ALT, alanine aminotransferase; AST, aspartate aminotransferase; HYP, hydroxyproline; MDA, malondialdehyde; SOD, superoxide dismutase; COL-1, collagen type 1; RT-qPCR, reverse transcription-quantitative polymerase chain reaction; ANOVA, analysis of variance.

and PTEN were overexpressed in activated HSC-T6 cells treated with RSV, the mRNA and protein expression of PTEN, as well as the protein expression of PI3K and p-AKT were decreased (all P<0.01; Fig. 6A and B). The HYP and MDA contents were decreased, while the SOD content was increased (Fig. 6C), and the COL-1 content was decreased (Fig. 6D).

Moreover, the mRNA and protein expression of α-SMA and TIMP-1 also decreased (Fig. 6E and F; all P<0.01).

Discussion

LF represents a protective response against chronic liver injury; however, incessant LF due to dysregulation results in liver cirrhosis and even hepatocellular carcinoma (33). Hepatocytes, immune and endothelial cells, macrophages and activated liver stellate cells jointly participate in the genesis of LF, which ultimately leads to chronic liver injury (3). RSV has been discovered to affect various biological features; for instance, it discourages inflammatory reactions, oxidative stress, apoptosis and mitochondrial function failure and promotes angiogenesis (34). In a previous study, RSV assisted in remedying liver diseases, including its effects on depressing necrosis, apoptosis and fat deposition caused by ischemia after liver transplantation; preventing liver injury from alcohol, cholestatic liver disease and chemicals; and modulating lipid and glucose metabolism to fight against liver steatosis and LF (35). In the present study, it was thus hypothesized that RSV may affect LF by inducing autophagy and activating the miR-20a-mediated PTEN/PI3K/AKT signaling pathway. Consequently, the data demonstrated that RSV suppressed LF progression.

First, the results of H&E and Masson's staining revealed that RSV attenuated rat LF. RSV, a type of dietary polyphenol found in grapes and red wine, exhibits the ability to protect the liver (36). It has been reported that RSV inhibits reactive oxygen species that are active players in the initiation of LF, thereby ameliorating LF malignancy (37). The present study revealed the ongoing development of autophagy in rats with LF resulting from RSV. Autophagy substantially participates in eliminating misfolded, aggregated and long-lived proteins, and impaired organelles and modulating growth, as it is closely related to the responses to a number of types of stress, including hypoxia, inflammation and endoplasmic reticulum stress (38). Autophagy induced by RSV is an essential step in the beneficial effect of RSV on inhibiting inflammation (39). As an essential protective factor, autophagy carries out an anti-inflammatory mechanism by phagocytizing pathogens, modulating T cell activation and controlling immune cell differentiation to hinder lipid peroxidation and oxidative stress to mitigate LF (40). In summary, RSV markedly alleviated LF.

Additionally, the present study revealed that RSV upregulated the PTEN/PI3K/AKT signaling pathway to suppress LF. As a variable phosphatase in human cancer, PTEN is an important participant in protein synthesis deregulation, cell growth and DNA activity (41). A previous study demonstrated that the loss of PTEN caused the overexpression of liver insulin and development of liver diseases, suggesting a positive role for PTEN in LF treatment (42). Evidence has indicated that the PI3K/AKT signaling pathway promotes T cell activation and inflammatory reactions to exacerbate ulcerative colitis (43). The deregulation of the PI3K/AKT signaling pathway is positively associated with metabolic function failure in liver diseases (44), which suggests that the PI3K/AKT signaling pathway may have a detrimental influence on LF treatment. The results from a previous study demonstrated that increased PTEN expression serves as a negative regulator of the PI3K/AKT signaling pathway through a series of biological activities (45).

The present study found that miR-20a suppressed PTEN expression. In lung cancer, the upregulated expression of miR-20a has emerged as an enhancer of cell growth, encouraging tumor development (46). In multiple myeloma, miR-20a directly targets PTEN, suppressing PTEN activity by reducing proliferation and promoting apoptosis (47). Notably, the present study found that RSV reversed the suppressive effects of miR-20a on PTEN. Functional assays revealed that RSV markedly decreased miR-20a expression and thus activated PTEN mRNA and protein expression, which was suppressed by miR-20a (20). Finally, RSV inhibited LF by downregulating miR-20a and upregulating the PTEN/PI3K/AKT signaling pathway. A previous study revealed a significant increase in miR-20a in liver-related diseases, suggesting that miR-20a functions as a convenient target in predicting LF (18). Generally, RSV was effective in blocking LF progression.

In conclusion, the present study supports the notion that RSV inhibits LF by inducing autophagy and activating the miR-20a-mediated PTEN/PI3K/AKT signaling pathway. These results reveal a novel strategy for the treatment of LF. Due to limitations in research funding and experimental conditions, the present study did not perform immunostaining to detectα-SMA. Furthermore, further investigations to determine whether cells in the exponential growth phase replicate physiological conditions in the liver are required. In the future, the authors aim to explore this aspect and further explore the mechanism of other targets of RSV via α-SMA immunostaining and focus more on seeking reliable therapeutic targets in LF. Nevertheless, although the findings of the present preclinical study have implications for the treatment of LF, these experimental results and the effective applications of RSV in clinical practice warrant further validation.

Acknowledgements

Not applicable.

Funding

The present study was financially supported by the Qian Ke He Platform Talent [grant no. (2018) 5779-26]; the Training Program of the National Natural Science Foundation of Affiliated Hospital of Guizhou Medical University (grant no. I-2020-20) and Doctoral Fund of Affiliated Hospital of Guizhou Medical University (grant no. I-20190-11).

Availability of data and materials

All the data generated or analyzed during this study are included in this published article.

Authors' contributions

All authors guarantee the integrity of the entire study. LZ, QM and MC conceived and designed the study. YW performed the experiments and acquired the data. ZZ analyzed and interpreted the data. All authors revised the manuscript for

important intellectual content and edited the manuscript. All authors read and approved the final manuscript.

Ethics approval and consent to participate

The present study was approved and supervised by the Ethics Committee of the Affiliated Baiyun Hospital of Guizhou Medical University. Every step in this experiment was approved by the laboratory animal ethics committee.

Patient consent for publication

Not applicable.

Competing interests

Not applicable.

References

1. Schuppan D, Ashfaq-Khan M, Yang AT and Kim YO: Liver fibrosis: Direct antifibrotic agents and targeted therapies. Matrix Biol 68-69: 435-451, 2018.
2. Zoubek ME, Trautwein C and Strnad P: Reversal of liver fibrosis: From fiction to reality. Best Pract Res Clin Gastroenterol 31: 129-141, 2017.
3. Campana L and Iredale JP: Regression of liver fibrosis. Semin Liver Dis 37: 1-10, 2017.
4. Altamirano-Barrera A, Barranco-Fragoso B and Mendez-Sanchez N: Management strategies for liver fibrosis. Ann Hepatol 16: 48-56, 2017.
5. Poilil Surendran S, George Thomas R, Moon MJ and Jeong YY: Nanoparticles for the treatment of liver fibrosis. Int J Nanomedicine 12: 6997-7006, 2017.
6. Petitclerc L, Gilbert G, Nguyen BN and Tang A: Liver fibrosis quantification by magnetic resonance imaging. Top Magn Reson Imaging 26: 229-241, 2017.
7. Sun M and Kisseleva T: Reversibility of liver fibrosis. Clin Res Hepatol Gastroenterol 39 Suppl 1: S60-S63, 2015.
8. Shi Y, Zhou J, Jiang B and Miao M: Resveratrol and inflammatory bowel disease. Ann N Y Acad Sci 1403: 38-47, 2017.
9. Hessin AF, Hegazy RR, Hassan AA, Yassin NZ and Kenawy SA: Resveratrol prevents liver fibrosis via two possible pathways: Modulation of alpha fetoprotein transcriptional levels and normalization of protein kinase C responses. Indian J Pharmacol 49: 282-289, 2017.
10. Liu C, Liao JZ and Li PY: Traditional Chinese herbal extracts inducing autophagy as a novel approach in therapy of nonalcoholic fatty liver disease. World J Gastroenterol 23: 1964-1973, 2017.
11. Li W, Zhang T, Guo L and Huang L: Regulation of PTEN expression by noncoding RNAs. J Exp Clin Cancer Res 37: 223, 2018.
12. Liang H, Wang X, Si C, Duan Y, Chen B, Liang H and Yang D: Downregulation of miR141 deactivates hepatic stellate cells by targeting the PTEN/AKT/mTOR pathway. Int J Mol Med 46: 406-414, 2020.
13. Petersen DR, Saba LM, Sayin VI, Papagiannakopoulos T, Schmidt EE, Merrill GF, Orlicky DJ and Shearn CT: Elevated Nrf-2 responses are insufficient to mitigate protein carbonylation in hepatospecific PTEN deletion mice. PLoS One 13: e0198139, 2018.
14. Dong Z, Li S, Wang X, Si L, Ma R, Bao L and Bo A: lncRNA GAS5 restrains CCl_4-induced hepatic fibrosis by targeting miR-23a through the PTEN/PI3K/Akt signaling pathway. Am J Physiol Gastrointest Liver Physiol 316: G539-G550, 2019.
15. Zhang DQ, Sun P, Jin Q, Li X, Zhang Y, Zhang YJ, Wu YL, Nan JX and Lian LH: Resveratrol regulates activated hepatic stellate cells by modulating NF-κB and the PI3K/Akt signaling pathway. J Food Sci 81: H240-H245, 2016.
16. Chai R, Fu H, Zheng Z, Liu T, Ji S and Li G: Resveratrol inhibits proliferation and migration through SIRT1 mediated posttranslational modification of PI3K/AKT signaling in hepatocellular carcinoma cells. Mol Med Rep 16: 8037-8044, 2017.
17. Zhu Q, Luo M, Zhou C, Chen Z, Huang W, Huang J, Zhao S and Yu X: Effect of danusertib on cell cycle, apoptosis and autophagy of hepatocellular carcinoma HepG2 cells in vitro. Nan Fang Yi Ke Da Xue Xue Bao 38: 1476-1484, 2018 (In Chinese).
18. Shrivastava S, Petrone J, Steele R, Lauer GM, Di Bisceglie AM and Ray RB: Up-regulation of circulating miR-20a is correlated with hepatitis C virus-mediated liver disease progression. Hepatology 58: 863-871, 2013.
19. Zhang Y, Zheng L, Ding Y, Li Q, Wang R, Liu T, Sun Q, Yang H, Peng S, Wang W and Chen L: MiR-20a induces cell radioresistance by activating the PTEN/PI3K/Akt signaling pathway in hepatocellular carcinoma. Int J Radiat Oncol Biol Phys 92: 1132-1140, 2015.
20. Dhar S, Kumar A, Rimando AM, Zhang X and Levenson AS: Resveratrol and pterostilbene epigenetically restore PTEN expression by targeting oncomiRs of the miR-17 family in prostate cancer. Oncotarget 6: 27214-27226, 2015.
21. Huang W, Li G, Qiu J, Gonzalez P and Challa P: Protective effects of resveratrol in experimental retinal detachment. PLoS One 8: e75735, 2013.
22. Saha L and Chakrabarti A: Understanding the anti-kindling role and its mechanism of Resveratrol in Pentylenetetrazole induced-kindling in a rat model. Pharmacol Biochem Behav 120: 57-64, 2014.
23. Zhan YY, Liang BQ, Li XY, Gu EM, Dai DP, Cai JP and Hu GX: The effect of resveratrol on pharmacokinetics of aripiprazole in vivo and in vitro. Xenobiotica 46: 439-444, 2016.
24. Zhang Y, Dong R, Yang Q, Zhang L, Li J and Zhao H: Resveratrol upregulates the gene and protein expressions of N-methyl-D-aspartate receptor 1 and protein kinase C in the hippocampus in Alzheimer's disease rats. Wei Sheng Yan Jiu 48: 269-278, 2019 (In Chinese).
25. Zatroch KK, Knight CG, Reimer JN and Pang DS: Refinement of intraperitoneal injection of sodium pentobarbital for euthanasia in laboratory rats (Rattus norvegicus). BMC Vet Res 13: 60, 2017.
26. Livak KJ and Schmittgen TD: Analysis of relative gene expression data using real-time quantitative PCR and the 2(-Delta Delta C(T)) method. Methods 25: 402-408, 2001.
27. Brunt EM: Grading and staging the histopathological lesions of chronic hepatitis: The Knodell histology activity index and beyond. Hepatology 31: 241-246, 2000.
28. Zhang XW, Mi S, Li Z, Zhou JC, Xie J, Hua F, Li K, Cui B, Lv XX, Yu JJ and Hu ZW: Antagonism of Interleukin-17A ameliorates experimental hepatic fibrosis by restoring the IL-10/STAT3-suppressed autophagy in hepatocytes. Oncotarget 8: 9922-9934, 2017.
29. Zou H, Wang T, Yuan J, Sun J, Yuan Y, Gu J, Liu X, Bian J and Liu Z: Cadmium-induced cytotoxicity in mouse liver cells is associated with the disruption of autophagic flux via inhibiting the fusion of autophagosomes and lysosomes. Toxicol Lett 321: 32-43, 2020.
30. Niu X, Fu N, Du J, Wang R, Wang Y, Zhao S, Du H, Wang B, Zhang Y, Sun D and Nan Y: MiR-1273g-3p modulates activation and apoptosis of hepatic stellate cells by directly targeting PTEN in HCV-related liver fibrosis. FEBS Lett 590: 2709-2724, 2016.
31. Cheng Y, Tian Y, Xia J, Wu X, Yang Y, Li X, Huang C, Meng X, Ma T and Li J: The role of PTEN in regulation of hepatic macrophages activation and function in progression and reversal of liver fibrosis. Toxicol Appl Pharmacol 317: 51-62, 2017.
32. Appourchaux K, Dokmak S, Resche-Rigon M, Treton X, Lapalus M, Gattolliat CH, Porchet E, Martinot-Peignoux M, Boyer N, Vidaud M, *et al*: MicroRNA-based diagnostic tools for advanced fibrosis and cirrhosis in patients with chronic hepatitis B and C. Sci Rep 6: 34935, 2016.
33. Bae M, Park YK and Lee JY: Food components with antifibrotic activity and implications in prevention of liver disease. J Nutr Biochem 55: 1-11, 2018.
34. Abu-Amero KK, Kondkar AA and Chalam KV: Resveratrol and ophthalmic diseases. Nutrients 8: 200, 2016.
35. Faghihzadeh F, Hekmatdoost A and Adibi P: Resveratrol and liver: A systematic review. J Res Med Sci 20: 797-810, 2015.
36. Tang L, Yang F, Fang Z and Hu C: Resveratrol ameliorates alcoholic fatty liver by inducing autophagy. Am J Chin Med 44: 1207-1220, 2016.
37. Zhao X, Li R, Liu Y, Zhang X, Zhang M, Zeng Z, Wu L, Gao X, Lan T and Wang Y: Polydatin protects against carbon tetrachloride-induced liver fibrosis in mice. Arch Biochem Biophys 629: 1-7, 2017.
38. Ravanan P, Srikumar IF and Talwar P: Autophagy: The spotlight for cellular stress responses. Life Sci 188: 53-67, 2017.

39. Park D, Jeong H, Lee MN, Koh A, Kwon O, Yang YR, Noh J, Suh PG, Park H and Ryu SH: Resveratrol induces autophagy by directly inhibiting mTOR through ATP competition. Sci Rep 6: 21772, 2016.
40. Ge MX, He HW, Shao RG and Liu H: Recent progression in the utilization of autophagy-regulating nature compound as anti-liver fibrosis agents. J Asian Nat Prod Res 19: 109-113, 2017.
41. Hopkins BD, Hodakoski C, Barrows D, Mense SM and Parsons RE: PTEN function: The long and the short of it. Trends Biochem Sci 39: 183-190, 2014.
42. He L, Gubbins J, Peng Z, Medina V, Fei F, Asahina K, Wang J, Kahn M, Rountree CB and Stiles BL: Activation of hepatic stellate cell in Pten null liver injury model. Fibrogenesis Tissue Repair 9: 8, 2016.
43. Chen Q, Duan X, Fan H, Xu M, Tang Q, Zhang L, Shou Z, Liu X, Zuo D, Yang J, *et al*: Oxymatrine protects against DSS-induced colitis via inhibiting the PI3K/AKT signaling pathway. Int Immunopharmacol 53: 149-157, 2017.
44. Matsuda S, Kobayashi M and Kitagishi Y: Roles for PI3K/AKT/PTEN pathway in cell signaling of nonalcoholic fatty liver disease. ISRN Endocrinol 2013: 472432, 2013.
45. Tsai CY, Wu JCC, Fang C and Chang AYW: PTEN, a negative regulator of PI3K/Akt signaling, sustains brain stem cardiovascular regulation during mevinphos intoxication. Neuropharmacology 123: 175-185, 2017.
46. Babu KR and Muckenthaler MU: MiR-20a regulates expression of the iron exporter ferroportin in lung cancer. J Mol Med (Berl) 94: 347-359, 2016.
47. Yuan J, Su Z, Gu W, Shen X, Zhao Q, Shi L, Jin C, Wang X, Cong H and Ju S: MiR-19b and miR-20a suppress apoptosis, promote proliferation and induce tumorigenicity of multiple myeloma cells by targeting PTEN. Cancer Biomark 24: 279-289, 2019.